

Large-area GaN n-core/p-shell arrays fabricated using top-down etching and selective epitaxial overgrowth

Sergiy Krylyuk,^{1,2} Dipak Paramanik,¹ Matt King,³ Abhishek Motayed,^{1,2,a)} Jong-Yoon Ha,^{1,2} John E. Bonevich,¹ Alec Talin,¹ and Albert V. Davydov¹

¹National Institute of Standards and Technology, Gaithersburg, Maryland 20899, USA

²Institute for Research in Electronics and Applied Physics, University of Maryland, College Park, Maryland 20742, USA

³Northrop Grumman Electronic Systems, Linthicum, Maryland 21090, USA

(Received 28 August 2012; accepted 14 November 2012; published online 14 December 2012)

We present large-area, vertically aligned GaN n-core and p-shell structures on silicon substrates. The GaN pillars were formed by inductively coupled plasma etching of lithographically patterned n-GaN epitaxial layer. Mg-doped p-GaN shells were formed using selective overgrowth by halide vapor phase epitaxy. The diameter of the cores ranged from 250 nm to 10 μ m with varying pitch. The p-shells formed truncated hexagonal pyramids with $\{1\bar{1}01\}$ side-facets. Room-temperature photoluminescence and Raman scattering measurements indicate strain-relaxation in the etched pillars and shells. Cross-sectional transmission electron microscopy revealed dislocation bending by 90° at the core-shell interface and reduction in their density in the shells. © 2012 American Institute of Physics. [<http://dx.doi.org/10.1063/1.4769376>]

GaN nanorod-based core-shell structures have gained significant attention in recent years due to their potential use in various optoelectronic devices.¹ These structures have significant benefits including large active surface area, enhanced light extraction efficiency, greater carrier confinement, and reduction of detrimental polarization effects. The latter benefit arises as p-n junctions can be realized on non-polar and semi-polar surfaces. GaN-based core-shell structures have been produced by a number of different techniques: (1) catalyst-assisted metal-organic vapor phase epitaxy (MOVPE),² (2) selective area epitaxy (SAE) of nanorods using MOVPE through a dielectric mask and subsequent conformal shell growth,^{3,4} and (3) combination of molecular beam epitaxy (MBE) grown n-type GaN nanowires and halide vapor phase epitaxy (HVPE) grown p-GaN conformal shells.⁵ For device implementations, such structures/growth-techniques must possess the following characteristics: high-aspect ratio, large-area uniformity in dimensions and orientation, scalable fabrication and growth methods, and precise control of shell morphology, microstructure, and dopant concentration. Although SAE⁶ appears to be the most promising approach in terms of achieving the desired dimensional and orientation control, it requires highly specific growth conditions leading to non-optimal material quality.⁷ Alternatively, the combination of nanopatterning and plasma etching to form GaN pillars and subsequent coaxial shell growth has been attempted to alleviate the problems of SAE.^{7,8} However, only limited attempts have been made to realize individual cores-shell structures and perform detailed microstructural and material characterization.

In this letter, we demonstrated dense arrays of vertically oriented, individual GaN core-shell structures realized with a combination of top-down etching of the n-type pillars and subsequent p-shell growth using selective epitaxy. Our approach is similar to the “pendeo-epitaxy” (PE) method demonstrated by Zheleva *et al.*⁹ However, instead of bars

oriented in particular crystallographic directions, we formed pillars with different shapes and dimensions by lithography and inductively coupled plasma (ICP) etching of GaN (0001) epitaxial film grown on Si substrates by MOVPE, followed by the epitaxial growth of Mg-doped shells using HVPE. Large-area arrays of such well-defined n-core/p-shell GaN structures could find their application in light-emitting and laser diodes, photodetectors, and solar cells. Moreover, due to high growth rates, HVPE “pendeo-epitaxy” (HVPE-PE) may be advantageous compared to the traditionally used MOVPE-based PE for growing thick GaN shells with reduced dislocation density.

The schematic of the GaN core-shell pillars fabrication process is detailed in Fig. 1. Si-doped n-GaN (0001) films were grown on Si (111) substrates in a commercial MOVPE reactor. First, Al_{1-x}Ga_xN buffer layer with varying x and thickness of ≈ 125 nm was grown on the Si substrate followed by deposition of 0.75 μ m thick GaN epilayer [Fig. 1(a)]. GaN wafers were patterned using deep UV lithography and metal liftoff. The etch-mask used for this study was Ti/Ni (50 nm/120 nm) deposited using electron-beam evaporation. The patterned samples were then etched in an ICP system using a Cl₂/N₂/Ar gas mixture with flow rates of 25/5/2 standard cubic centimeters per minute (sccm). The ICP source power and RF power were set at 1000 W and 500 W, respectively. The etching time was adjusted to provide complete removal of the unmasked GaN layer with subsequent removal of about 0.5 μ m of the underlying Si substrate [Fig. 1(b)]. After the ICP processing, the metal etch mask was removed in HF:HNO₃:H₂O (1:1:10) solution followed by deionized water rinse and nitrogen blow dry. GaN pillars of three different cross-sections, circles, squares, and diamonds, were formed with lateral dimensions ranging from 10 μ m to 250 nm and pitches ranging from 20 μ m to 0.5 μ m. The edges/vertexes of the square/diamond pillars were aligned along the GaN $\langle 1\bar{1}00 \rangle$ and $\langle 11\bar{2}0 \rangle$ directions. Mg-doped GaN shells were epitaxially grown over the

^{a)}Electronic mail: amotayed@nist.gov.

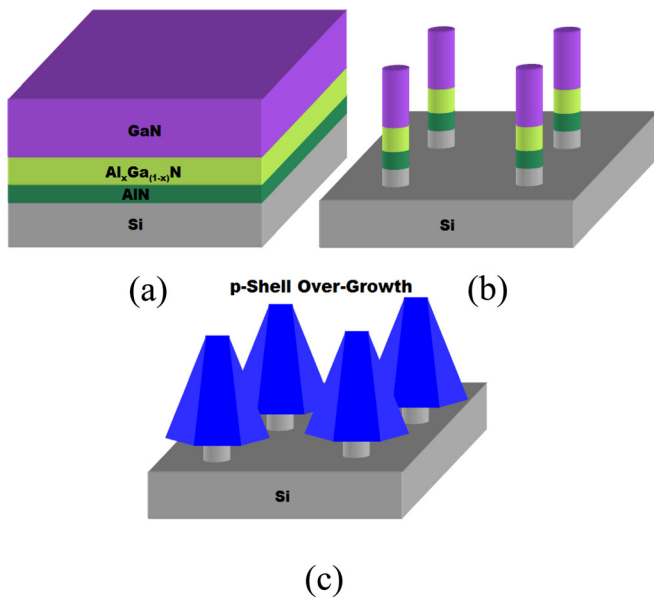


FIG. 1. Schematic representation of the fabrication process of GaN core-shell structure: (a) as-grown layer structure, (b) pillar formation by ICP etching, and (c) after p-GaN shell overgrowth.

etched GaN pillars [Fig. 1(c)] in a custom-built horizontal HVPE reactor. The overgrowth was performed at 980 °C to 1040 °C and 60 k Pa (450 Torr). The GaCl_x precursor gaseous species were synthesized by reacting HCl gas (6 sccm to 20 sccm) with molten Ga at 700 °C. Ammonia at 200 sccm to 1500 sccm was used as the group V precursor and N₂ (5000 sccm) was the carrier gas. The Mg source for the p-type doping was biscyclopentadienyl-magnesium (Cp₂Mg). Post-growth activation of Mg-dopants was conducted in a rapid thermal annealing system at 750 °C for 15 min in Ar.

After the growth, the samples were examined using a scanning electron microscope (SEM) and transmission elec-

tron microscope (TEM). Cross-sectional TEM samples were prepared by site specific *in situ* lift-out methods in a focused ion beam (FIB) instrument and subsequently observed in a 300 kV TEM instrument. Room-temperature photoluminescence (PL) and Raman scattering were collected using a 325 nm He-Cd laser and a 532 nm frequency doubled Nd:YAG laser excitation sources, respectively, and a high resolution spectrometer with an 800 nm focal length.

A representative SEM image of an array of the etched GaN pillars with initial diameter of 0.75 μm and 2.5 μm pitch is shown in Fig. 2(a). Because of etch-mask erosion, the final tip diameters of the circular and square pillars were reduced to ≈0.5 μm, and that of the diamond pillars to ≈0.44 μm, all with ≈80° tapering angle. The etched pillars had 0.9 μm of GaN on top of 0.5 μm of Si. Fig. 2(b) shows the orientation of the different cross-section pillars relative to the GaN crystallographic directions. Irrespective of the initial size/shape of GaN pillars, the HVPE overgrowth produced truncated hexagonal pyramids for all growth conditions employed in this study [Figs. 2(b)–2(e)]. The top c-plane facet progressively diminishes as the overgrowth proceeds. The side facets have a distinct ~62° angle from the horizontal indicating that they are formed by {11̄01} planes (Fig. 3). The obtained core-shell pyramids are similar to those grown by SAE through dot-patterned dielectric masks on GaN films.¹⁰ It is well-recognized that for both PE and epitaxial lateral overgrowth (ELO) of GaN, different side facets may appear depending on growth conditions and/or shape and orientation of GaN “seeds.”^{10,11} In particular, different vertical and slanted facets are observed in both MOVPE and HVPE ELO of GaN if the stripe mask patterns are aligned along the ⟨11̄00⟩ or ⟨11̄20⟩ direction. However, our overgrowth procedure always yielded {11̄01} facets, even for the round-shaped pillars (leftmost image in Fig. 2(b)), the square-shaped pillars with nominally etched {11̄00} and {11̄20}

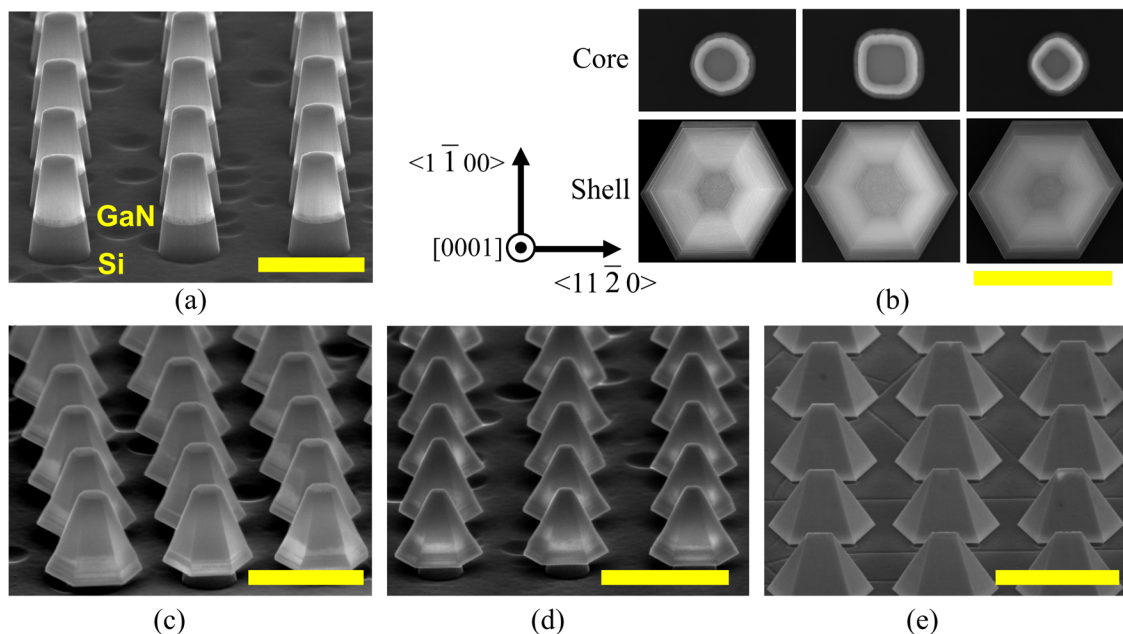


FIG. 2. SEM images of (a) array of as-etched GaN pillars with 0.5 μm diameter and 2.5 μm pitch; (b) circle-, square-, and diamond-shaped pillars before and after p-shell growth (plan-view); (c) and (d) p-shells grown for 10 min at 1020 °C and HCl/NH₃ flow rates of 6/200 (sccm) on (c) 0.5 μm and (d) 0.2 μm pillars; (e) p-shells grown for 5 min at 1040 °C and HCl/NH₃ flow rates of 20/1500 (sccm) on square pillars with 10 μm width and 20 μm pitch. Tilted SEM images were taken at 70°. The scale bars are 2 μm for (a)–(d) and 20 μm for (e).

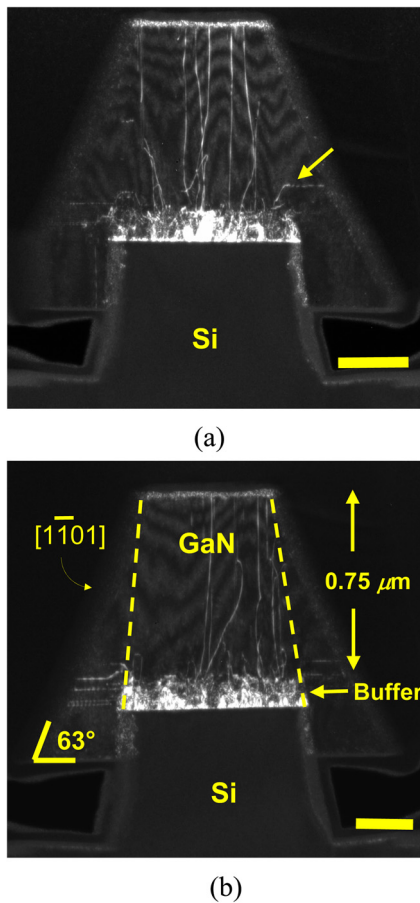


FIG. 3. Dark-field cross-sectional TEM images of two different core-shell structures with original square core with diameter $0.5 \mu\text{m}$ in (a) and (b). The cross-sections were prepared using FIB instrument. The arrow in (a) points to the bending of a dislocation as it crosses into the shell. Dashed lines in (b) outline the shape of the initial GaN core. The scale bar is $0.2 \mu\text{m}$ in both the images.

sidewalls (center image in Fig. 2(b)), or the diamond-shaped pillars with other low-indexed sidewalls (rightmost image in Fig. 2(b)). The evolution of $\{1\bar{1}01\}$ inclined facets rather than $\{1\bar{1}00\}$ vertical facets might have been induced by the initial tapering of the as-etched pillars. The preference for the non-vertical sidewall formation is also consistent with Ref. 12, where GaN pillars always terminated with inclined $\{1\bar{1}01\}$ facets when non-hydrogen carrier gas was used in the HVPE system.

The cross-sectional dark-field TEM images of the core-shell pillars are shown in Fig. 3. Note that the growing shell extends below the original interface between GaN film and Si substrate. The growth rate appears to be higher for the bottom plane of the GaN shell than its top (0001) surface. Since no GaN was deposited on the Si substrate due to the selectivity of HVPE process, this growth enhancement is tentatively assigned to diffusion of the reactants from the Si surface toward GaN pillars.¹³ It is evident from Fig. 3 that dislocations in the pillars do not propagate vertically into the shells. Most of the observed dislocations bent by 90° from their initial propagation direction when they reached the $\{1\bar{1}01\}$ facets and finally propagated parallel to the basal plane in the shells. Threading dislocations commonly observed in GaN are of three types: (1) edge dislocations with Burgers vector $b = \pm \langle 11\bar{2}0 \rangle$, screw dislocations with $b = \pm \langle 0001 \rangle$, and

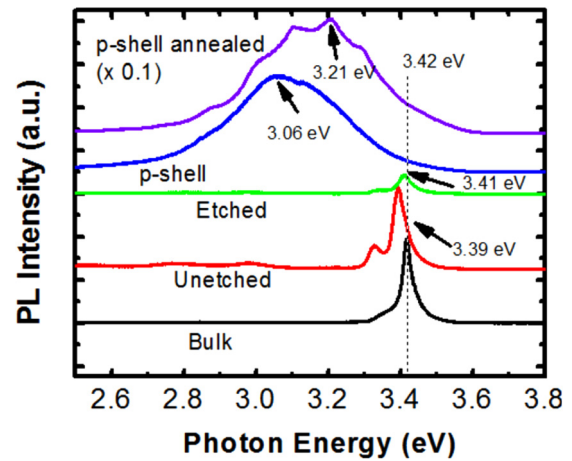


FIG. 4. Room-temperature PL spectra of bulk GaN (black), unetched thin film (red), etched pillars (green), after p-shell growth (blue), and after the activation anneal (magenta). The dashed line indicates the peak position of room-temperature NBE of strain-free GaN. The etched sample showed significant reduction in the intensity. The PL intensity of activated p-shell increased by a factor of 10, when compared to the as-grown shell.

mixed dislocations with $b = \pm \langle 11\bar{2}0 \rangle \pm \langle 0001 \rangle$. Bending of dislocations has been often observed in ELO of GaN.¹⁴ The energy of a dislocation depends on its Burgers vector and its propagation direction, which is dictated by energy minimization.¹⁵ For the edge dislocations, the propagation direction with minimum energy is parallel to its Burgers vector, which would correspond to a 90° bend, converting an edge dislocation into a pure screw dislocation.

The room-temperature PL spectra of the GaN epilayer, etched pillars, and overgrown shells (before and after Mg activation) are shown in Fig. 4. For comparison, we also plotted the PL spectra from a free-standing, stress-free 3 mm thick GaN sample grown by HVPE method. For the etched pillars and the p-shells, the spectra were taken from the $10 \mu\text{m}$ diameter structures to enhance the intensity of the peaks, although the trend is similar for smaller diameter structures. At room-temperature, the near-band edge (NBE) transition observed in GaN has been attributed to band-to-band recombination as well as to excitonic recombination.¹⁶ The thin GaN epilayer clearly exhibits a tensile-strain induced 30 meV red-shift of the NBE emission peak, as compared to the bulk NBE peak. This is in agreement with reports on GaN thin-film grown on Si substrate, where the GaN is under biaxial tensile-strain.¹⁷ The peak at 3.33 eV present in the un-etched sample has been observed in the PL spectra of GaN grown on Si, and is often attributed to the donor acceptor pair (DAP) transitions.^{18,19} The 20 meV blue-shift of the NBE emission of the etched sample indicates partial strain-relaxation due to etching. Such blue-shift in PL has also been observed for etched GaN nanocolumns on Si.²⁰ Growth of the Mg-doped p-shell substantially changes the emission characteristics as seen in Fig. 4, with the disappearance of the NBE peak and evolution of broad emission centered at 3.06 eV for the as-grown shell. Activation annealing of the shell at 750°C in Ar resulted in an increase in the overall intensity with the emission peak blueshifted to 3.21 eV. In MOVPE grown Mg-doped GaN, the 2.95 eV emission band is thought to be due to conduction band to

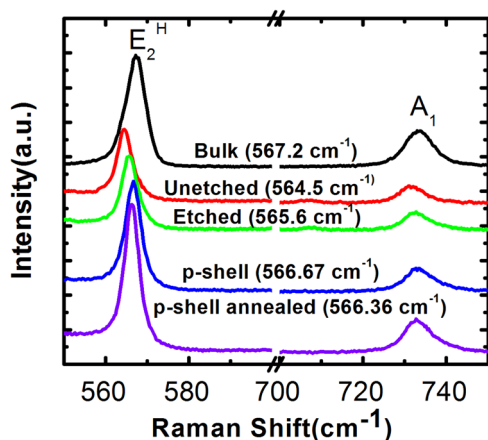


FIG. 5. Room-temperature Raman scattering spectra from bulk GaN (black), unetched thin film (red), etched pillars (green), after p-shell growth (blue), and after the Mg activation anneal (magenta). The position of E_2^H is given in parenthesis.

deep-level (or complexes) transitions, and the 3.21 eV emission band is due to conduction band to shallow Mg acceptor level transitions.²¹ This agrees well with the observed results, i.e., in the case of the as-deposited shell the Mg complexes might dominate the PL, whereas after the activation anneal the shallow acceptors dominate the transitions.

The biaxial strain in hexagonal GaN is most conveniently probed through the E_2^H phonon mode in Raman scattering, as it is most sensitive to biaxial strain in c-plane and is the most intense.²² Fig. 5 shows the room-temperature Raman scattering spectra in the back-scattering geometry from the unetched GaN thin film, 10 μm diameter circular pillars, after p-type shell growth, and after Mg-activation anneal. For comparison, the Raman spectrum from the 3 mm thick bulk GaN is also shown. Compared to the standard value of strain-free E_2^H peak (567.6 cm^{-1}),²³ the as-grown GaN on Si exhibits tensile strain, evident in the red-shifted (3.5 cm^{-1}) E_2^H peak. The blue-shift (1.1 cm^{-1} from the unetched sample) of the E_2^H peak after plasma etching is in agreement with the PL results, indicating the partial strain relaxation due to etching. Assuming the stress coefficient for the Raman shift for the E_2^H mode for GaN on Si is $2.9\text{ cm}^{-1}\text{ GPa}^{-1}$,²² we can compute a relaxation of 0.37 GPa in the 10 μm diameter pillars due to etching. Further blue shifting of the E_2^H peak due to the shell growth might be due to the compressive effect of the conformal epitaxial growth, where the GaN core is hydrostatically compressed by the shell.

We have demonstrated vertically aligned GaN core-shell structures using a combination of top-down etching and selective area shell growth on the etched pillars. As-etched pillars clearly showed strain-relaxation manifested in blue-shift in both PL and Raman scattering spectra. Following the epitaxial shell overgrowth, the strain was further reduced. The cross-sectional TEM of the core-shell structures revealed reduction in dislocation density in the shells. The

present structures have potential for applications as photodetectors, light-emitters, and field-emitters requiring large-area arrays of nanoscale sub-components.

The nanostructures were fabricated at the Nanofab clean room of the NIST Center for Nanoscale Science and Technology. Authors thank Dr. Kil-Won Moon of NIST for preparing the TEM samples and Dr. Erich Walter of NIST for his help with the PL setup. The University of Maryland portion of the work was partially supported by the Defense Threat Reduction Agency, Basic Research Award No. HDTRA1-10-1-0107.

¹S. Li and A. Waag, *J. Appl. Phys.* **111**, 071101 (2012).

²F. Qian, S. Gradečak, Y. Li, C.-J. Wen, and C. M. Lieber, *Nano Lett.* **5**, 2287 (2005).

³Y. J. Hong, C.-H. Lee, A. Yoon, M. Kim, H.-K. Seong, H. J. Chung, C. Sone, Y. J. Park, and G.-C. Yi, *Adv. Mater.* **23**, 3284 (2011).

⁴A. Waag, X. Wang, S. Fündling, J. Ledig, M. Erenburg, R. Neumann, M. A. Suleiman, S. Merzsch, J. Wei, S. Li, H. H. Wehmann, W. Bergbauer, M. Straßburg, A. Trampert, U. Jahn, and H. Riechert, *Phys. Status Solidi C* **8**, 2296 (2011).

⁵A. Sanders, P. Blanchard, K. Bertness, M. Brubaker, C. Dodson, T. Harvey, A. Herrero, D. Rourke, J. Schlager, S. Sanford, A. N. Chiamonti, A. Davydov, A. Motayed, and D. Tsvetkov, *Nanotechnology* **22**, 465703 (2011).

⁶S. D. Hersee, X. Sun, and X. Wang, *Nano Lett.* **6**, 1808 (2006).

⁷G. T. Wang and Q. Li, "Nanowires: Lighting the future," SPIE Newsroom, July 26, 2011, doi: 10.1117/2.1201106.003796.

⁸N. A. Fichtenbaum, C. J. Neufeld, C. Schaake, Y. Wu, M. H. Wong, M. Grundmann, S. Keller, S. P. Denbaars, J. S. Speck, and U. K. Mishra, *Jpn. J. Appl. Phys., Part 2* **46**, L230 (2007).

⁹T. S. Zheleva, S. A. Smith, D. B. Thomson, K. J. Linthicum, P. Rajagopal, and R. F. Davis, *J. Electron. Mater.* **28**, L5 (1999).

¹⁰For a review, see, e.g., P. Gibart, *Rep. Prog. Phys.* **67**, 667 (2004).

¹¹O. Chelda-Gourmal, A. Trassoudaine, Y. Andre, S. Bouchoule, E. Gil, J. Touret, D. Castelluci, and R. Cadoret, *J. Cryst. Growth* **312**, 1899 (2010).

¹²H.-P. Liu, J.-D. Tsay, W.-Y. Liu, Y.-D. Guo, J. T. Hsu, and In.-G. Chen, *J. Cryst. Growth* **260**, 79 (2004).

¹³C. C. Mitchell, M. E. Coltrin, and J. Han, *J. Cryst. Growth* **222**, 144 (2001).

¹⁴M. D. Craven, S. H. Lim, F. Wu, J. S. Speck, and S. P. Denbaars, *Appl. Phys. Lett.* **81**, 1201 (2002).

¹⁵S. Gradečak, P. Stadelmann, V. Wagner, and M. Illegems, *Appl. Phys. Lett.* **85**, 4648 (2004).

¹⁶E. F. Schubert, I. D. Goepfert, W. Grieshaber, and J. M. Redwing, *Appl. Phys. Lett.* **71**, 921 (1997).

¹⁷D. G. Zhao, S. J. Xu, M. H. Xie, S. Y. Tong, and H. Yang, *Appl. Phys. Lett.* **83**, 677 (2003).

¹⁸G. P. Yablonskii, E. V. Lutsenko, V. N. Pavlovskii, V. Z. Zubialevich, A. L. Gurskii, H. Kalisch, A. Szymakowski, R. A. Jansen, A. Alam, Y. Dikme, B. Schineller, and M. Heuken, *Phys. Status Solidi A* **192**, 54 (2002).

¹⁹L. T. Tung, K. L. Lin, E. Y. Chang, W. C. Huang, Y. L. Hsiao, and C. H. Chiang, *J. Phys.: Conf. Ser.* **187**, 012021 (2009).

²⁰N. Thilloen, K. Sebald, H. Hardtdegen, R. Meijers, R. Calarco, S. Montanari, N. Kaluza, J. Gutowski, and H. Lüth, *Nano Lett.* **6**, 704 (2006).

²¹M. Smith, G. D. Chen, J. Y. Lin, H. X. Jiang, A. Salvador, B. N. Sverdlov, A. Botchkarev, H. Morko, and B. Goldenber, *Appl. Phys. Lett.* **68**, 1883 (1996).

²²H. Harima, *J. Phys.: Condens. Matter* **14**, R967 (2002).

²³V. Y. Davydov, Y. E. Kitaev, I. N. Goncharuk, A. N. Smirnov, J. Graul, O. Semchinova, D. Uffman, M. B. Smirnov, A. P. Mirgorodsky, and R. A. Evarestov, *Phys. Rev. B* **58**, 12899 (1998).